JOURNAL OF GEOPHYSICAL RESEARCH, VOL. 106, NO. D10, PAGES 10,223–10,232, MAY 27, 2001

Horizontal velocity structure functions in the upper troposphere and lower stratosphere 1. Observations

John Y. N. Cho
Department of Earth, Atmospheric, and Planetary Sciences, Massachusetts Institute of Technology, Cambridge, Massachusetts

Erik Lindborg
Department of Mechanics, Kungl Tekniska Högskolan, Stockholm, Sweden

Abstract. We compute horizontal velocity structure functions using quasiglobal data accumulated by specially equipped commercial aircraft on 7630 flights from August 1994 to December 1997. Using the ozone concentration measurements, we classify the results as tropospheric or stratospheric. We further divide the results into four absolute latitude bands. For separation distance r between 10 and 100 km, the lower stratospheric diagonal third-order structure functions are proportional to negative r. This implies a downscale energy cascade, and we estimate the mean energy dissipation rate to be $\langle\epsilon\rangle \approx 6\times10^{-5}$ m^2 s^{-3}. For r between 300 and 1500 km, a positive r^3 dependence was visible for the polar stratospheric data. This may be the result of a two-dimensional (2D) turbulence downscale enstrophy cascade, and we estimate the average enstrophy flux to be $\Pi_\omega \approx 2\times10^{-15}$ s^{-3} and the energy spectral constant to be $\mathcal{K} \approx 2$. The negative sign of these third-order functions at mesoscales in both the upper troposphere and lower stratosphere provide no support for an inverse energy cascade 2D turbulence. At scales above ~100 km, the second-order structure functions increase with latitude in the troposphere and decrease with latitude in the stratosphere. The off-diagonal third-order functions in the stratosphere show a remarkably clean negative r^2 dependency from 10 to 1000 km in scale.

1. Introduction

For over two decades the physics underlying the atmospheric kinetic energy spectrum has remained in controversy. At mesoscales, where the horizontal wave number (k) spectrum has a $k^{-5/3}$ form, two types of theories have emerged: stratified turbulence [*Gage*, 1979; *Lilly*, 1983] and gravity-wave cascade [*Dewan*, 1979]. Subsequent comparisons of the theories with data have not yielded a consensus on which better describes nature [*Gage and Nastrom*, 1986; *Vincent and Eckermann*, 1990; *Bacmeister et al.*, 1996; *Cho et al.*, 1999a; *Högström et al.*, 1999]. The case for stratified turbulence using numerical simulations has been reviewed by *Lilly et al.* [1998], while *Koshyk et al.* [1999] has pushed the spatial resolution of a general circulation model to produce a $k^{-5/3}$ spectrum at mesoscales. At larger scales, where the spectrum turns to a k^{-3} dependence, quasigeostrophic turbulence [*Charney*, 1971] is generally cited as the physical mechanism. The turbulence hypotheses are based on the two-dimensional (2D) theory of *Kraichnan* [1967] with the assumption of both a large-scale and a small-scale source of energy [*Lilly*, 1989]. However, even for the large-scale regime, there are dissenting ideas such as enhancement in energy at low wave numbers due to inertial modes [*Gardner et al.*, 1993] and the Bose condensation effect [*Smith and Yakhot*, 1994], which also lead to the observed spectral form [e.g., *Nastrom and Gage*, 1985].

Clearly, the Fourier power spectrum alone cannot distinguish between the various theories. Spectral methods also have difficulty dealing with data gaps and uneven sampling, and great care must be taken to avoid spectral leakage especially with "red noise" type of data [e.g., *Dewan and Grossbard*, 2000]. Structure functions do not have such problems and are easily computed. Recently theoretical third-order velocity structure functions for 2D turbulence were derived and compared to extensive observations made by specially equipped commercial aircraft [*Lindborg*, 1999] (hereafter L99). The results showed a narrow range (~30–300 km) in which the third-order structure functions were positive, consis-

Paper number 2000JD900814.
0148-0227/01/2000JD900814$09.00

tent with the downscale enstrophy cascade of 2D turbulence. Unfortunately, however, a wrong sign in one line in the data analysis program, resulted in an erroneous third-order structure function, while the results for the second- and fourth-order structure functions were not affected by this bug. The conclusions in L99, based on this calculation of the third-order structure function, must therefore be revised. The new results are more easily interpreted as direct evidence of a forward energy cascade. About the same time as the error was discovered, E. Lindborg was contacted by J. Y. N. Cho, who had developed a similar program to compute structure functions from the same data set. After the error had been removed from Lindborg's program, the two programs showed very similar results. Another limitation in L99 was that the data set was not subdivided with respect to regions, such as high versus low latitudes and troposphere versus stratosphere, that could have quite different dynamical characteristics. In fact, the wind data from the measurement of ozone and water vapor by Airbus in-service aircraft (MOZAIC) program [*Marenco et al.*, 1998] used by L99 covers a wide range of latitudes and longitudes as well as quite a bit of the lower stratosphere. Therefore we wished to recompute the structure functions with a corrected program and to explore their dependency on various parameters. The calculations presented in this paper were made with the program developed by J. Y. N. Cho. The new findings that we present in this paper have prompted corresponding theoretical developments that are put forth in the companion paper (hereafter Part 2) [*Lindborg and Cho*, this issue].

2. Structure Function Analysis

We closely followed the procedure outlined by L99. However, there were some differences such as the following. First our data consisted of a somewhat expanded MOZAIC set (August 1994 to December 1997, 7630 flights), whereas L99 used August 1994 to April 1997 with 5754 flights. Second, in order to avoid variability caused by rapid changes in altitude, we specified that the pairs of points used for the structure function computations lie within the same standard flight level. There were five flight levels from 9.4 to 11.8 km, each spaced 600 m apart. The adherence to the standard levels were quite strict [*Thouret et al.*, 1998]. Third we used the ozone measurement to differentiate between the troposphere and stratosphere. If the ozone levels associated with the pair of data points were both under 100 ppbv (parts per billion by volume), then the result was binned as tropospheric. If the ozone concentrations for the data-point pair were both over 200 ppbv, then the result was classified as stratospheric. If one point was in the troposphere and the other point was in the stratosphere, the result was not included in either group. The two thresholds were chosen from the ozone concentration histograms for MOZAIC cruise levels [*Thouret et al.*, 1998]. (Of course, our data set was limited to the upper troposphere and lower stratosphere, but for brevity we will refer simply to tropospheric and stratospheric data in this paper.) Finally, we divided the data-point pairs according to four latitudinal bands: 0°–10°, 10°–30°, 30°–50°, and 50°–70° for the troposphere and 30°–40°, 40°–50°, 50°–60°, and 60°–70° for the stratosphere, where the number used was the absolute value of the average of the latitudes at the two points. There were few points in the stratosphere equatorward of 30°, since the tropical tropopause was usually above the flight altitude. For a schematic of the flight route distributions, see *Cho et al.* [1999b].

There are multiple ways of defining the tropopause (e.g., the lapse rate, the cold point, potential vorticity equal to some constant, composition change), and each method has its own strengths and weaknesses. The ozone concentration as a delimiter has some ambiguities where there is vigorous exchange across the tropopause. However, by employing two values, less than 100 ppbv for the troposphere and greater than 200 ppbv for the stratosphere, we hope to have avoided much of this ambiguity.

Note also that because the latitude-longitude coordinates for the Air France aircraft data were purposely

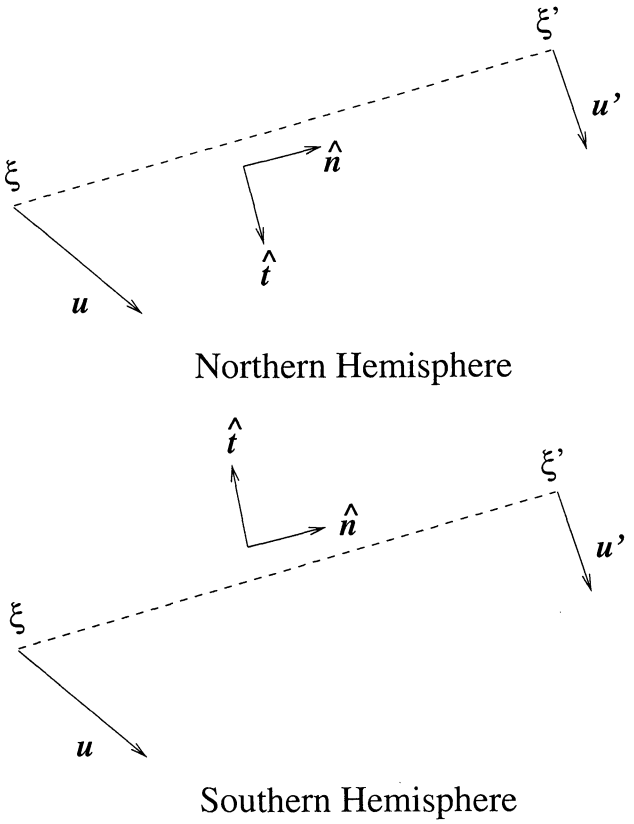

Figure 1. Illustration of the longitudinal and transverse direction definitions. The point indicated by ξ' is further along the flight path than the point indicated by ξ. For this example, u_L and u'_L are positive for both hemispheres, while u_T and u'_T are positive in the Northern Hemisphere and negative in the Southern Hemisphere.

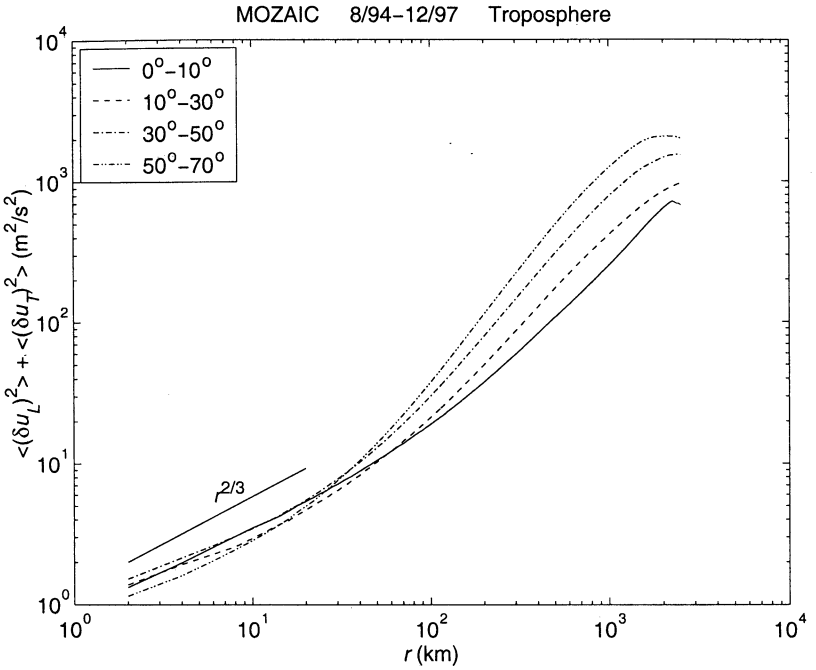

Figure 2. Sum of the tropospheric longitudinal and transverse second-order horizontal velocity structure functions versus latitude. Latitudes are absolute values.

degraded to about a 1-min resolution (a result of pilot union concerns), we linearly interpolated the position to the original 4-s resolution. This was also done by L99 but was not stated in the paper. The data from the other airlines (Sabena, Lufthansa, and Austrian Airlines) were not altered.

Next we briefly describe the computational procedure. The velocity structure function is defined by $\langle(\delta u)^m\rangle$, where m is the order and the angle brackets denote ensemble averaging. Here $\delta u \equiv u' - u$ is the difference in horizontal velocity components between two points $\boldsymbol{\xi}'$ and $\boldsymbol{\xi}$. We will calculate structure functions for the longitudinal and transverse components, u_L and u_T, of the horizontal velocity. We define these orthogonal components in the following way. Let $\hat{\mathbf{n}} = (\boldsymbol{\xi}' - \boldsymbol{\xi})/|\boldsymbol{\xi}' - \boldsymbol{\xi}|$ and $\hat{\mathbf{e}}$ be the upward pointing vertical unit vector. Then $u_L(\boldsymbol{\xi}) = \mathbf{u}(\boldsymbol{\xi}) \cdot \hat{\mathbf{n}}$ and $u_T(\boldsymbol{\xi}) = \mathbf{u}(\boldsymbol{\xi}) \cdot \hat{\mathbf{t}}$, where $\hat{\mathbf{t}} = \hat{\mathbf{n}} \times \hat{\mathbf{e}}$ in the Northern

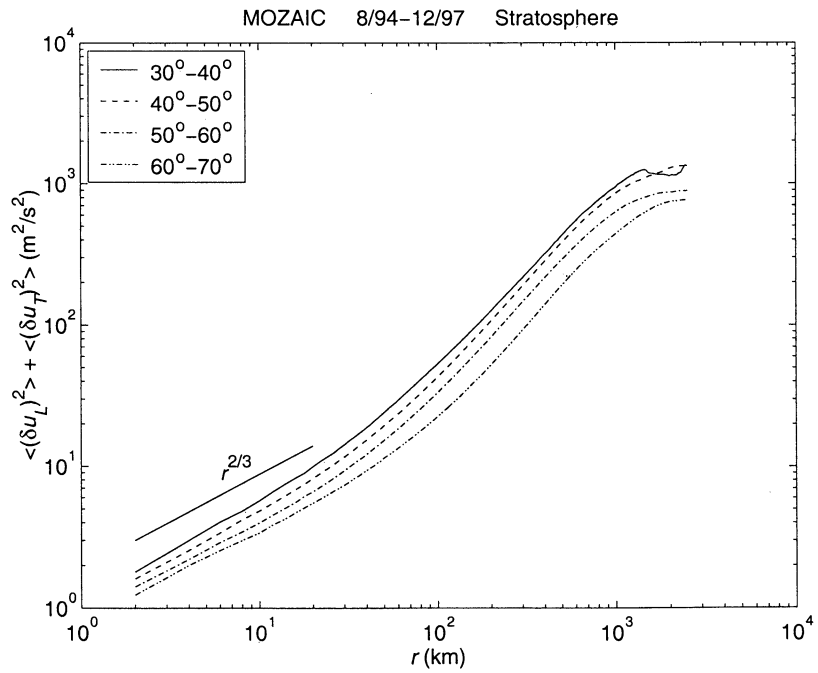

Figure 3. Same as Figure 2, except for the stratosphere.

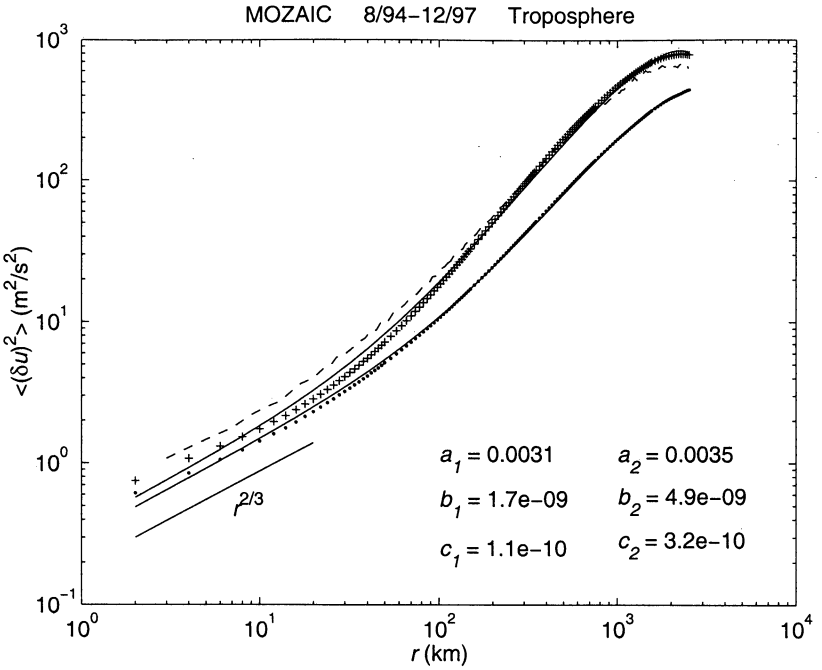

Figure 4. Second-order horizontal velocity structure functions for the longitudinal (dots) and transverse (crosses) components calculated for tropospheric data. The solid lines are nonlinear least squares fits to the theoretical functions; the values of the fitted parameters are displayed in the lower right-hand corner. The dashed line is the theoretical isotropic transverse function calculated from the measured longitudinal function.

Hemisphere and $\hat{\mathbf{t}} = \hat{\mathbf{e}} \times \hat{\mathbf{n}}$ in the Southern Hemisphere. This definition avoids cancellation of rotational effects when both hemispheric data are summed together. We omitted cross-equatorial data pairs from the structure function calculations to avoid the sign reversal of the transverse component at the equator. A graphical illustration of the vector definitions is shown in Figure 1.

The separation distance $r = |\boldsymbol{\xi}' - \boldsymbol{\xi}|$, where $\boldsymbol{\xi}'$ is further along the flight path than $\boldsymbol{\xi}$, was calculated using the latitude-longitude coordinates, the altitudes, and an elliptical polar model of the Earth radius, $R = AB/(1 - B\cos\phi)$, where $A = 1.896 \times 10^6$ km, $B = 3.353 \times 10^{-3}$, and ϕ is latitude. The separation distance was taken to be the shortest arc length not the straight-line distance. Following L99 we used a set of 140 separation distances between 2 and 2510 km. For every data point the other end point was found by searching through the rest of the flight for the point coming closest to the specified r. If that distance was not within 1 km of the specified r, then the velocity difference was not computed.

2.1. Second-Order Structure Functions

One of the immediately striking results was the latitudinal dependence of the second-order structure functions. The tropospheric results are shown in Figure 2. While there was no clear latitudinal dependence at mesoscales, for $r \gtrsim 100$ km the sum of the longitudinal and transverse second-order functions increased monotonically with latitude. The equivalent plot for the stratosphere is shown in Figure 3. Here the latitudinal dependence was reversed; furthermore, the function followed the same trend at all length scales. Similar large-scale latitudinal tendencies for both the troposphere and stratosphere were observed in the kinetic energy spectra by *Nastrom and Gage* [1985]. *Gage and Nastrom* [1986] attributed the tropospheric increase in spectral power with latitude to a geometric effect, i.e., that the spectra were computed in rectilinear coordinates rather than against hemispheric wave number. They adjusted their results by a factor of $\cos\phi$ to get a more constant value with latitude but an even stronger dependency in the stratosphere. We do not think this procedure is justified since, first, the $\cos\phi$ factor should be applied as a length-scale correction (not directly to the spectral power) and, second, the expectation of constant energy at a given hemispheric wave number leads to a pile-up of energy at the poles. Although we cannot explain this tropospheric latitudinal dependency fully at this time, we propose some ideas on the line of attack for this problem in Part 2.

Since the second-order structure function is in Fourier duality with the power spectrum, if the function follows a power law, r^α, then $\beta = \alpha + 1$, where $k^{-\beta}$ is the corresponding horizontal wave number power spectrum. This relationship is valid for $1 < \beta < 3$ (signal with stationary increments) [*Davis et al.*, 1996], a criterion that was satisfied in this case. Note that the stratospheric curves closely followed $r^{2/3}$ at small scales, which corresponds to $k^{-5/3}$ in the Fourier domain.

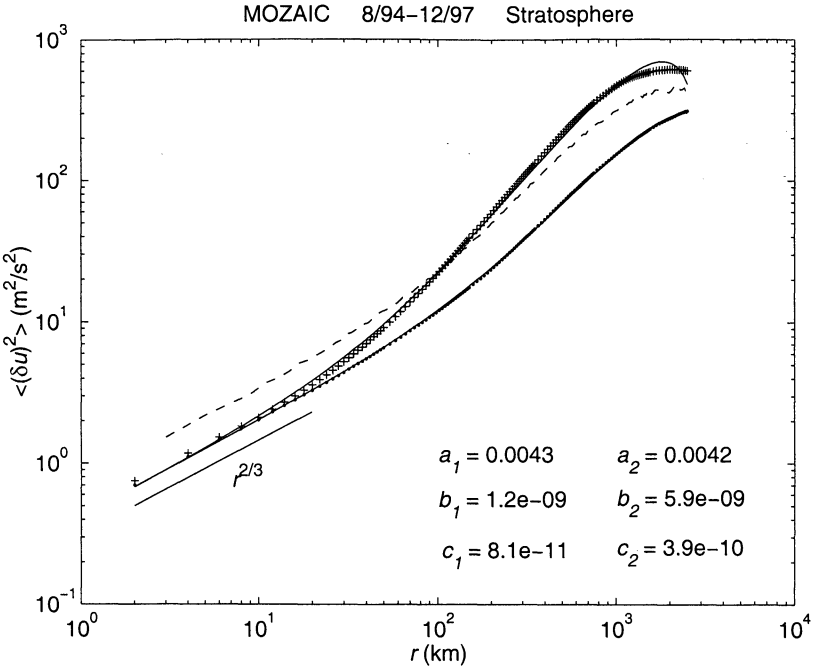

Figure 5. Same as Figure 4, except for stratospheric data.

Figure 4 shows the longitudinal (dots) and transverse (crosses) second-order velocity structure functions separately for tropospheric data. The solid lines are fits to the theoretical second-order structure functions given by L99:

$$\left\langle (\delta u_L)^2 \right\rangle = a_1 r^{2/3} + b_1 r^2 - c_1 r^2 \ln r \qquad (1)$$

and

$$\left\langle (\delta u_T)^2 \right\rangle = a_2 r^{2/3} + b_2 r^2 - c_2 r^2 \ln r \ . \qquad (2)$$

The values of the fitted parameters are shown in Figure 4. The dashed line is the theoretical 2D isotropic transverse function calculated from the measured longitudinal function using the relation

$$\left\langle (\delta u_T)^2 \right\rangle = \frac{\mathrm{d}}{\mathrm{d}r} \left[r \left\langle (\delta u_L)^2 \right\rangle \right] \qquad (3)$$

derived by L99. The stratospheric second-order structure functions are shown in Figure 5.

An interesting difference between the tropospheric and stratospheric structure functions is the comparison with the theoretical 2D isotropy relation. In the stratosphere the measured functions were farther from isotropy than in the troposphere at all scales except around 100 km. The approach to 2D isotropy can be quantified by inserting (1) into (3) and equating the result to (2). We then see that for assumed isotropy, the constants for the transverse second-order structure function are $a_{2Iso} = 5a_1/3$, $b_{2Iso} = 3b_1 - c_1$, and $c_{2Iso} = 3c_1$. We can compare these values to the fitted parameters of the measured transverse function by forming ratios. The results, along with all the fitted parameters, are shown in Tables 1 and 2 for all the data subsets. Note that a_2/a_{2Iso} is associated with the $\sim r^{2/3}$ regime at mesoscales, while b_2/b_{2Iso} and c_2/c_{2Iso} are associated with the $\sim r^2$ regime at longer scales.

Table 1. Tropospheric Horizontal Velocity Second-Order Structure Function Parameters

Parameter	0°–10°	10°–30°	30°–50°	50°–70°	All
a_1 (10^{-3} m$^{2/3}$ s^{-2})	2.9	2.9	3.4	2.8	3.1
b_1 (10^{-9} s^{-2})	0.42	1.0	1.9	2.7	1.7
c_1 (10^{-10} s^{-2})	0.26	0.65	1.2	1.7	1.1
a_2 (10^{-3} m$^{2/3}$ s^{-2})	4.5	3.6	3.8	2.7	3.5
b_2 (10^{-9} s^{-2})	0.89	2.3	4.7	9.0	4.9
c_2 (10^{-10} s^{-2})	0.55	1.5	3.1	5.9	3.2
a_2/a_{2Iso}	0.93	0.74	0.67	0.58	0.68
b_2/b_{2Iso}	0.72	0.78	0.84	1.1	0.98
c_2/c_{2Iso}	0.71	0.77	0.86	1.2	0.97

Table 2. Stratospheric Horizontal Velocity Second-Order Structure Function Parameters

Parameter	30°–40°	40°–50°	50°–60°	60°–70°	All
a_1 (10^{-3} m$^{2/3}$ s^{-2})	5.6	5.0	4.1	3.6	4.3
b_1 (10^{-9} s^{-2})	2.2	1.7	1.2	0.73	1.2
c_1 (10^{-10} s^{-2})	1.5	1.1	0.80	0.47	0.81
a_2 (10^{-3} m$^{2/3}$ s^{-2})	5.9	4.7	4.0	3.4	4.2
b_2 (10^{-9} s^{-2})	9.4	7.9	5.9	3.2	5.9
c_2 (10^{-10} s^{-2})	6.3	5.3	4.0	2.1	3.9
a_2/a_{2Iso}	0.63	0.56	0.59	0.57	0.59
b_2/b_{2Iso}	1.5	1.6	1.7	1.5	1.7
c_2/c_{2Iso}	1.4	1.6	1.7	1.5	1.6

The most striking difference in the ratios was between the troposphere and stratosphere at long scales. We see that b_2/b_{2Iso} and c_2/c_{2Iso} were clearly larger in the stratosphere than in the troposphere. The other major difference was in the latitudinal trends in the troposphere and stratosphere. Even accounting for the narrower range of latitudes in the stratosphere, one can see that the ratios were more-or-less independent of latitude. In the troposphere, a_2/a_{2Iso} decreased with latitude, while b_2/b_{2Iso} and c_2/c_{2Iso} increased with latitude.

2.2. Third-Order Structure Functions

The third-order structure function can be decomposed into four parts: $\langle(\delta u_L)^3\rangle$, $\langle\delta u_L(\delta u_T)^2\rangle$, $\langle(\delta u_L)^2\delta u_T\rangle$, and $\langle(\delta u_T)^3\rangle$. We shall call the first two terms diagonal and the latter two terms off-diagonal, nomenclature arising from the corresponding tensor notation. For the diagonal terms, L99 derived the following relation for 2D turbulence:

$$\left\langle(\delta u_L)^3\right\rangle + \left\langle\delta u_L\,(\delta u_T)^2\right\rangle = 2P_S r + \frac{1}{4}Q_L r^3\,, \qquad (4)$$

where P_S is the energy input power of a small-scale force and Q_L is the enstrophy input power of a large-scale force. The positive signs of the right-hand terms imply a negative spectral energy flux and a positive enstrophy flux through Fourier space.

The calculated diagonal third-order functions are shown in Plates 1a and 1b. Perhaps the most significant result here was the negative r dependence at scales of ~10–100 km for the overall stratospheric data (solid line, with red indicating negative sign). The implication is that this was a downscale energy inertial subrange and that the mean energy dissipation rate $\langle\epsilon\rangle$ could be estimated from it. We performed a least squares fit of the absolute value of the data to r in log-log space for $10 < r < 150$ km to obtain $\langle\epsilon\rangle \approx 6\times10^{-5}$ m^2 s^{-3} for the stratosphere. Because the overlay of data from different latitudinal bands makes it difficult to see the negative r regime in Plate 1b, we plot only the overall stratospheric data in Figure 6. The fit to an r dependency in the interval $10 < r < 150$ km is shown as a straight line. Note the negative sign of the data in this regime as indicated by circles. See Part 2 for further details and for estimates of the energy spectral constants. The tropospheric data could not be well fit with a negative r law. Past midlatitude climatological estimates of $\langle\epsilon\rangle$ in the altitude region of 9–12 km range from $\sim9\times10^{-5}$ to $\sim3\times10^{-4}$ m^2 s^{-3} using in situ balloon observations [*Fukao et al.*, 1994] and radar Doppler spectral width data [*Nastrom and Eaton*, 1997], so our estimate does not differ greatly. In fact, a collection of other more episodic in situ measurements shows a typical value closer to $\sim 10^{-5}$ m^2 s^{-3} [*Dewan*, 1997]. Note that these previous measurements were made in the three-dimensional (3D) turbulence inertial subrange.

At scales greater than 100 km, the behavior of the functions differed between the troposphere and stratosphere. The overall tropospheric data yielded a roughly negative r^2 law, while the overall stratospheric data had a subrange that was positive with an arguably r^3 dependence. This latter dependence was most clearly seen in the 60°–70° absolute latitude band. This supports the possibility of a downscale enstrophy inertial cascade at large scales in the stratosphere, especially in the polar region. Since the average enstrophy flux $\Pi_\omega = Q_L$, we can fit equation (48) from Part 2 in a least squares sense in log-log space to the data to extract $\Pi_\omega \approx 1\times10^{-15}$ s^{-3} for the overall stratosphere ($540 < r < 1400$ km) and $\Pi_\omega \approx 2\times10^{-15}$ s^{-3} for the polar stratosphere ($290 < r < 1500$ km). The fitting procedure was the same as the one used previously for Figure 6. The fit is shown in Figure 7. These values agree well with an early estimate of $\sim 10^{-15}$ s^{-3} given by *Charney* [1971]. Furthermore, by nonlinear least squares fittings of equation (66) of L99 to the measured second-order functions and using the above values for Π_ω, one can get $\mathcal{K}$, which is a constant in the enstrophy inertial range energy spectrum $E(k) = \mathcal{K}\Pi_\omega^{2/3}k^{-3}$. We obtain $\mathcal{K} \approx 5$ for the overall stratosphere and $\mathcal{K} \approx 2$ for the polar stratosphere. The latter value is reasonably close to unity and is comparable to the *Leith and Kraichnan* [1972] model estimate of 1.74.

However, we must caution that latitudinal inhomogeneities may strongly affect (perhaps even dominate)

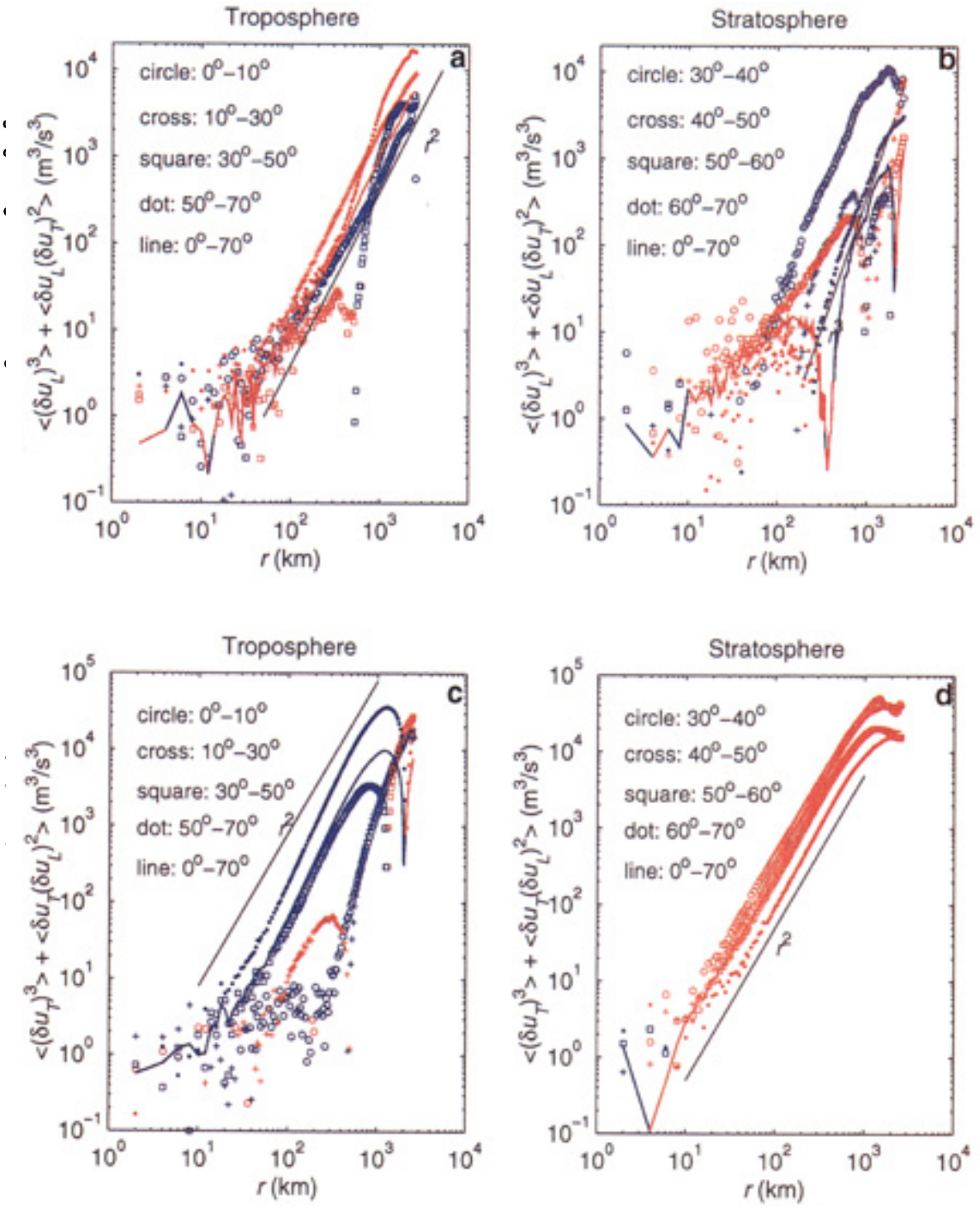

Plate 1. Sum of the diagonal third-order horizontal velocity structure functions for (a) tropospheric and (b) stratospheric data and sum of the off-diagonal third-order horizontal velocity structure functions for (c) tropospheric and (d) stratospheric data. Blue indicates positive sign, and red indicates negative sign. Symbols for the different latitude bands are indicated in the legend. Black lines corresponding to an r^2 or r^3 dependency are shown as guides to the eye.

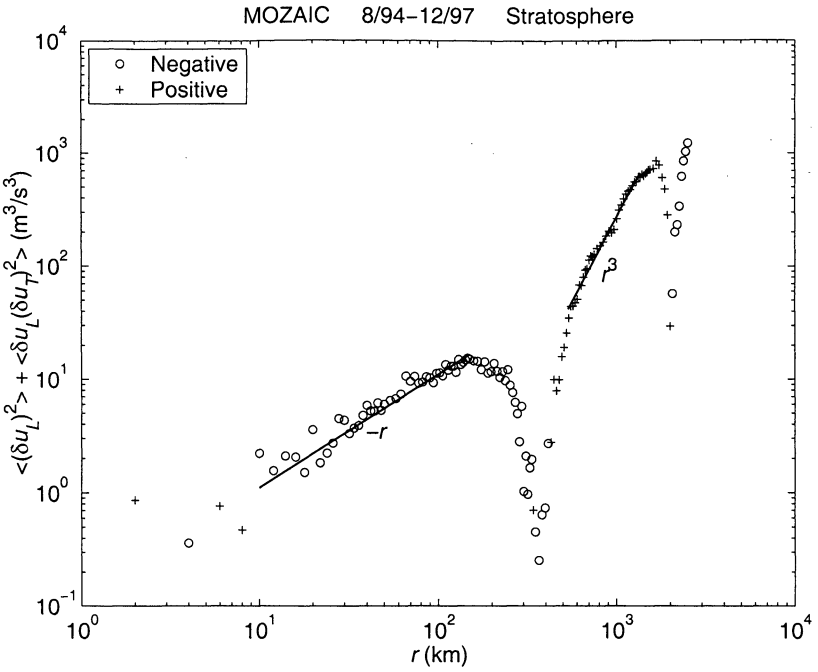

Figure 6. Plot showing a fit of $-r$ for $10 < r < 150$ km and r^3 for $540 < r < 1400$ km to the sum of the measured stratospheric diagonal third-order functions. Straight lines are fits to $-r$ and r^3 in the respective subranges. Circles and crosses indicate negative and positive values, respectively.

the third-order functions results. These concerns are addressed in more detail in Part 2.

We also calculated the off-diagonal terms, which are shown in Plates 1c and 1d. The convergence was apparently better than for the diagonal terms. The most remarkable result here was the consistency of the stratospheric functions, which followed a negative r^2 law in the interval ~10–1000 km at all latitudes. The tropospheric functions, however, were mostly positive with variable power law dependencies. Another intrigu-

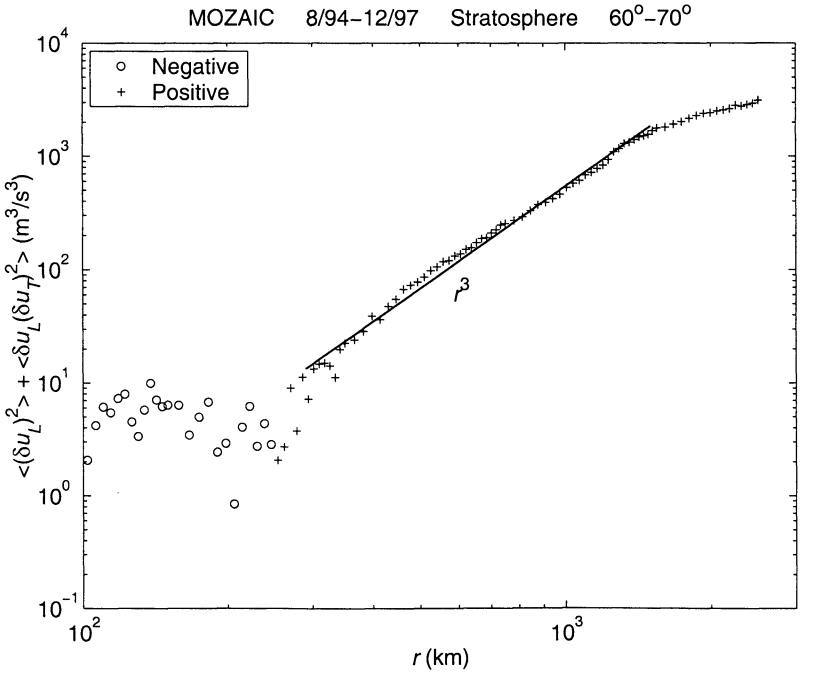

Figure 7. Plot showing a fit of r^3 to the sum of the measured polar stratospheric diagonal third-order functions for $290 < r < 1500$ km. The straight line is a least squares fit in log-log space to r^3 in the displayed range. Circles and crosses indicate negative and positive values, respectively.

ing feature was the tendency of the two off-diagonal terms to balance each other, thus leading to a kind of geostrophic balance. This will be shown and discussed in Part 2.

3. Summary Discussion

What can we glean from these results? We believe that the most significant result was the clear emergence of a negative r dependence in the stratospheric diagonal third-order structure functions for separation distances between 10 and 100 km. This contradicted the existence of an inverse energy cascade at mesoscales in the lower stratosphere and, instead, indicated a downscale energy cascade. As shown by L99 (and also in Part 2), an inverse cascade would have given us a positive linear third-order structure function. From theoretical considerations presented in Part 2 [*Lindborg and Cho*, this issue] we estimated $\langle\epsilon\rangle \approx 6 \times 10^{-5}$ m^2 s^{-3}, which was entirely consistent with other estimates of $\langle\epsilon\rangle$ in this height regime. These stratospheric results lend support to theories that require a downscale energy flow, such as the gravity-wave cascade theory [*Dewan*, 1979, 1997]. The overall tropospheric diagonal third-order functions were also negative at these scales, but we could not conclude that the functional form was r because of the poor convergence of the results.

At larger scales, the positive r^3 dependence of the diagonal third-order functions expected for the downscale enstrophy cascade of 2D turbulence was only clearly visible in the polar stratospheric data (for $300 < r < 1500$ km). (There was also a narrower subrange visible in the overall stratospheric data.) We estimated the corresponding mean enstrophy flux to be $\Pi_\omega \approx 2 \times 10^{-15}$ s^{-3} and the energy spectral constant to be $\mathcal{K} \approx 2$, both reasonable values. Whether the apparent lack of a positive r^3 dependence in the other regional subsets means that 2D turbulence was not effective in those regions is not clear. Large-scale inhomogeneities can affect (perhaps dominate) the third-order functions, as will be discussed in Part 2.

As for the off-diagonal third-order functions, the emergence of a balance between the two components implying a kind of geostrophic balance will be discussed in Part 2. At this time we are unable to explain the remarkably clean negative r^2 dependency from 10 to 1000 km in scale for the stratosphere. This topic will be taken up in a future study.

The relative clarity of the stratospheric results compared to those from the troposphere reminds us of the importance of the tropopause as a dynamical barrier. Owing to the suppression of vertical motion, 2D assumptions are bound to be better satisfied in the stratosphere. Even though our large data set was restricted to a narrow altitude region (~9–12 km), the structure function characteristics were markedly different below and above the tropopause. Conversely, one must be aware that simplified dynamical models that are effective in the stratosphere may be quite insufficient in the troposphere where vertical motions play a crucial role in a wide range of scales. However, the lack of evidence for an inverse energy cascade bodes well for numerical models in general, since unresolved subgrid-scale processes are not likely to alter the energetics of the larger scale dynamics.

Acknowledgments. The MIT work was funded by NASA grant NAG1-2306. The KTH work was supported by the Swedish Research Council for Engineering Sciences. We would also like to thank the MOZAIC program for use of their data, especially Alain Marenco and Valérie Thouret. MOZAIC was funded in part by the European Communities (DG XII-C, DG XII-D) with strong support from Airbus Industrie and its partners, Air France, Lufthansa, Austrian Airlines, and Sabena.

References

Bacmeister, J. T., S. D. Eckermann, P. A. Newman, L. Lait, K. R. Chan, M. Loewenstein, M. H. Proffitt, and B. L. Gary, Stratospheric horizontal wavenumber spectra of winds, potential temperature, and atmospheric tracers observed by high-altitude aircraft, *J. Geophys. Res.*, *101*, 9441–9470, 1996.

Charney, J. G., Geostrophic turbulence, *J. Atmos. Sci.*, *28*, 1087–1095, 1971.

Cho, J. Y. N., R. E. Newell, and J. D. Barrick, Horizontal wavenumber spectra of winds, temperature, and trace gases during the Pacific Exploratory Missions, 2, Gravity waves, quasi-two-dimensional turbulence, and vortical modes, *J. Geophys. Res.*, *104*, 16,297–16,308, 1999a.

Cho, J. Y. N., R. E. Newell, V. Thouret, A. Marenco, and H. G. Smit, Trace gas study accumulates forty million frequent-flyer miles for science, *Eos Trans. AGU*, *80*, 377, 383–384, 1999b.

Davis, A., A. Marshak, W. Wiscombe, and R. Cahalan, Scale invariance of liquid water distributions in marine stratocumulus, Part I, Spectral properties and stationarity issues, *J. Atmos. Sci.*, *53*, 1538–1558, 1996.

Dewan, E. M., Stratospheric wave spectra resembling turbulence, *Science*, *204*, 832–835, 1979.

Dewan, E., Saturated-cascade similitude theory of gravity wave spectra, *J. Geophys. Res.*, *102*, 29,799–29,817, 1997.

Dewan, E. M., and N. Grossbard, Power spectral artifacts in published balloon data and implications regarding saturated gravity wave theories, *J. Geophys. Res.*, *105*, 4667–4684, 2000.

Fukao, S., M. D. Yamanaka, N. Ao, W. K. Hocking, T. Sato, M. Yamamoto, T. Nakamura, T. Tsuda, and S. Kato, Seasonal variability of vertical eddy diffusivity in the middle atmosphere, 1, Three-year observations by the middle and upper atmosphere radar, *J. Geophys. Res.*, *99*, 18,973–18,987, 1994.

Gage, K. S., Evidence for a $k^{-5/3}$ law inertial range in mesoscale two-dimensional turbulence, *J. Atmos. Sci.*, *36*, 1950–1954, 1979.

Gage, K. S., and G. D. Nastrom, Spectrum of atmospheric vertical displacements and spectrum of conservative scalar passive additives due to quasi-horizontal atmospheric motions, *J. Geophys. Res.*, *91*, 13,211–13,216, 1986.

Gardner, C. S., C. A. Hostetler, and S. J. Franke, Gravity wave models for the horizontal wave number spectra of atmospheric velocity and density fluctuations, *J. Geophys. Res.*, *98*, 1035–1049, 1993.

Högström, U., A.-S. Smedman, and H. Bergström, A case study of two-dimensional stratified turbulence, *J. Atmos. Sci.*, *56*, 959–976, 1999.

Koshyk, J. N., K. Hamilton, and J. D. Mahlman, Simulation of the $k^{-5/3}$ mesoscale spectral regime in the GFDL SKYHI general circulation model, *Geophys. Res. Lett.*, *26*, 843–846, 1999.

Kraichnan, R. H., Inertial ranges in two-dimensional turbulence, *Phys. Fluids*, *10*, 1417–1423, 1967.

Leith, C. E., and R. H. Kraichnan, Predictability of turbulent flows, *J. Atmos. Sci.*, *29*, 1041–1058, 1972.

Lilly, D. K., Stratified turbulence and the mesoscale variability of the atmosphere, *J. Atmos. Sci.*, *40*, 749–761, 1983.

Lilly, D. K., Two-dimensional turbulence generated by energy sources at two scales, *J. Atmos. Sci.*, *46*, 2026–2030, 1989.

Lilly, D. K., G. Bassett, K. Droegemeier, and P. Bartello, Stratified turbulence in the atmospheric mesoscales, *Theor. Comp. Fluid Dyn.*, *11*, 139–153, 1998.

Lindborg, E., Can the atmospheric kinetic energy spectrum be explained by two-dimensional turbulence?, *J. Fluid Mech.*, *388*, 259–288, 1999.

Lindborg, E., and J. Y. N. Cho, Horizontal velocity structure functions in the upper troposphere and lower stratosphere, 2, Theoretical considerations, *J. Geophys. Res.*, this issue.

Marenco, A., et al., Measurement of ozone and water vapor by Airbus in-service aircraft: The MOZAIC airborne program, An overview, *J. Geophys. Res.*, *103*, 25,631–25,642, 1998.

Nastrom, G. D., and F. D. Eaton, Turbulence eddy dissipation rates from radar observations at 5-20 km at White Sands Missile Range, NM, *J. Geophys. Res.*, *102*, 19,495–19,505, 1997.

Nastrom, G. D., and K. S. Gage, A climatology of atmospheric wavenumber spectra of wind and temperature observed by commercial aircraft, *J. Atmos. Sci.*, *42*, 950–960, 1985.

Smith, L. M., and V. Yakhot, Finite-size effects in forced two-dimensional turbulence, *J. Fluid Mech.*, *274*, 115–138, 1994.

Thouret, V., A. Marenco, P. Nédélec, and C. Grouhel, Ozone climatologies at 9–12 km altitude as seen by the MOZAIC airborne program between September 1994 and August 1996, *J. Geophys. Res.*, *103*, 25,653–25,679, 1998.

Vincent, R. A., and S. D. Eckermann, VHF radar observations of mesoscale motions in the atmosphere: Evidence for gravity wave Doppler shifting, *Radio Sci.*, *25*, 1019–1037, 1990.

J. Y. N. Cho, Department of Earth, Atmospheric, and Planetary Sciences, Massachusetts Institute of Technology, 77 Massachusetts Avenue, Room 54-1823, Cambridge, MA 02139-4307. (jcho@pemtropics.mit.edu)

E. Lindborg, Department of Mechanics, KTH, S-100 44 Stockholm, Sweden. (erikl@mech.kth.se)

(Received April 7, 2000; revised October 17, 2000; accepted November 7, 2000.)